Performance enhancement of a vibration energy harvester via harmonic time-varying damping: A pseudospectral-based approach

Performance enhancement of a vibration energy harvester via harmonic time-varying damping: A pseudospectral-based approach

Article *in* Mechanical Systems and Signal Processing · August 2021

DOI: 10.1016/j.ymssp.2021.108331

CITATIONS
0

READS
31

2 authors:

Giuseppe Giorgi
Politecnico di Torino
55 PUBLICATIONS **756** CITATIONS
SEE PROFILE

Nicolás Faedo
Politecnico di Torino
42 PUBLICATIONS **298** CITATIONS
SEE PROFILE

Highlights

Performance enhancement of a vibration energy harvester via harmonic time-varying damping: A pseudospectral-based approach

Giuseppe Giorgi, Nicolás Faedo

- A vibration energy harvester with harmonic time-variations of the damping coefficient.
- Energy-maximization optimal control problem framed via pseudospectral approach.
- Different combinations of zero-, first-, and second- order harmonics are studied.
- Bandwidth and efficiency of active and semi-active control strategies are compared.
- The best control law has both sine and cosine terms at twice the excitation frequency.

Performance enhancement of a vibration energy harvester via harmonic time-varying damping: A pseudospectral-based approach

Giuseppe Giorgi[a], Nicolás Faedo[a]

[a]*MOREnergy Lab, Department of Mechanical and Aerospace Engineering, Politecnico di Torino, 10129 Torino, Italy*

Abstract

Energy harvesting technologies are attracting increasing attention in the last decades, mainly thanks to the rapid advancement of sensors miniaturization, wireless sensors network, the internet of things, and the growing awareness on energy efficiency. The main objective of current research on energy harvesters is to enlarge the natural response bandwidth in order to increase the otherwise insufficient performance away from resonance. While popular approaches consider the inclusions of specific nonlinearities, this paper investigates the benefits of time variations of the damping coefficient of a linear power take-off system. A rigorous mathematical framework is firstly introduced, based on optimal control and pseudospectral decomposition, providing proofs and conditions for the existence of an unique optimal solution. Furthermore, a convenient algebraic formulation for the calculation of the steady-state response is provided, applicable to a wider family of time-varying systems. Such a tool is used to extensively study harmonic variations of the control damping parameters, discussing various combinations of orders and orthogonal terms. The optimization is first performed unconstrained, then forcing passivity, hence considering both active and semi-active controls. It is found that, in both cases, the best performance is achieved with damping variations at twice the exciting frequency, including both cosine and sine terms in the control law, while lower and higher harmonics are of less relevance.

Keywords: Vibration energy harvester, linear time-variant system, pseudospectral approach, active control, semi-active control, energy-maximization optimal control.

1. Introduction

The development of engineering products has always focused on optimizing the performance of a system in achieving its objective, minimizing costs, energy consumption, operation time, wear on components, just to mention a few representative metrics. In last decades, such an optimization is more and more relying on a pervasive sensorization, in order to make systems more intelligent and inform the underlying control logic. Such a trend encompasses all scales, from micro-level systems, such as bio-engineering appliances [1], macro-level, such as condition monitoring, fault-tolerant control and predictive maintenance for large mechanical systems [2], and network-level, such as holistic management of medium-high voltage national electricity grid [3]. This recent development pathway has been enabled by the rapid advancement of wireless sensors network (WSN) [4], micro electro-mechanical systems (MEMS) [5], and the success of the Internet of Things (IoT) [6]. The current mature industrial standard is based on state-of-the-art batteries or wired connections, both affected by inherent limitations: on the one hand, batteries have limited and stringent energy density, restricted life cycle, may imply hazardous disposal, and require periodic replacement and

labour cost, particularly costly in remote locations or in health implants [7]; on the other hand, wired connections may become not economical or practical due to the cost of wire materials, increasing electricity resistance and eventually connection difficulties for dynamic devices [8].

Thanks to latest developments, driving costs down and efficiencies up, an attractive alternative solution is offered by energy harvesting (EH) technologies, also known as energy scavengers. The vision is to exploit available (free) energy from the environment, and convert it into useful electrical energy to power sensors and/or charge batteries. EHs have the potential to guarantee reliable and continuous power supply, lower installation and maintenance costs, and enable solitary sensors and spread network applications. In the field of mechanical systems, vibration energy harvesters (VEHs) are becoming particularly popular, since vibration is essentially ubiquitous [9]; moreover, VEH can contribute to generate energy while also eliminating undesired vibrations, detrimental for long-term structural integrity [10]. The most common and mature VEH concepts are based on electromagnetic (EM) or piezoelectric (PE) conversion systems: EM is more suitable than PE for low frequencies (lower than 20 Hz [11]), typical of transport, building, and large mechanical systems in general. Moreover, EM have higher conversion efficiencies and no external voltage source is required. Despite a lower output voltage, higher power and current outputs are achieved, thanks to particularly low impedance [11].

Vibration sources are abundant in the environment, but often broadband or noisy. Simple linear VEH are normally very performant only at their natural resonance frequency, while the response abruptly degrades at any different frequency. Therefore, in order to become economical and convenient, structural performance enhancement of VEHs needs to be introduced, aimed at both power amplitude magnification and broadening of the frequency bandwidth. Popular expedients are to introduce nonlinearities in the system by operating with its architecture [12]: Duffing nonlinearity [13], bistability [14], parametric oscillators [15] and stochastic oscillators [16], among others. An other, less beaten, track envisions the use of linear time variant (LTV) systems instead, in order to obtain either active or semi-active control strategies. *Active* control strategies are expected to generate the highest mean power, but a bidirectional energy flow is required between the vibrator and the transducer, hence usually more expensive and complex machineries. Examples of active control strategies for VEH are found in optimal stochastic control [17], including nonlinearities [18], in piezoelectric circuits [19] via appropriate tension control across the piezoelectric transducer [20], or considering positive/negative parametric resonance [21]. Electromagnetic transducers can be easily used, as long as they are designed to permit bidirectional power flow, including H-Bridge architecture and bidirectional DC-DC or DC-AC converters [22]. The open question, under a techno-economic point of view, is if the marginal increase in cost and complexity is compensated by a greater gain in converted power. A hybrid solution is realized by *semi-active* control strategies, that refer to an active alteration of a passive system parameter, so that no explicit actuator is required [23]. Such mechanisms can be implemented, for example, via variable orifice dampers (with an external actuator modifying the diameter of the orifice [24]), controllable fluid dampers [25]), or magneto-rheological dampers (where the viscosity of the magnetic fluid is controlled via tuning of the electric field [26]). Although the energy required by semi-active control strategy is typically negligible with respect to the requirements of active strategies, they both normally need the presence of an energy storage device.

This paper focuses on VEH at low frequency (about 1 Hz), hence applicable to relatively large mechanical systems and transport application, using an electromechanical power take-off (PTO) module. However, the presented methodology is general and applicable to a large class of

systems, fulfilling a set of mild assumptions. Performance enhancement, in terms of both frequency bandwidth and response amplitude, is sought via LTV systems, where the PTO damping coefficient is variable in time. In particular, based on results in the literature (see, for instance, [25], [21], and [27]) harmonic variations of the damping coefficient are assumed, considering a mono-chromatic external excitation.

The contributions of this study are explicitly discussed in the following paragraphs. Inspired by the approximation framework presented in [28] to compute the response of autonomous systems, and [29] for finite-dimensional transcription of optima control problems, the first fundamental novelty is to propose a rigorous and formal mathematical framework based on a steady-state approach to optimal control of energy harvesters, where the control objective is, effectively, energy-maximization. In particular, existence and uniqueness of periodic solutions for the controlled energy harvester are firstly guaranteed, under a set mild assumptions. Since a closed-form expression for the steady-state mapping is virtually impossible to compute (given the intrinsic non-autonomous nature of the PTO damping), an approximation technique based on a pseudospectral approach is proposed[1], allowing the computation of the steady-state response of the energy harvester with an arbitrary degree of accuracy, and close to no computational burden (since is given as the solution of an algebraic equation). Furthermore, conditions for existence and uniqueness of such an approximation are explicitly derived and discussed, being this crucial for practical implementations. Finally, the approximating steady-state response is used to transcribe the infinite-dimensional optimal control problem, associated with energy-maximization, to a finite-dimensional nonlinear program, which can be solved efficiently by means of state-of-the-art numerical routines. This has a tangible consequence on the practical implementation of proposed control laws, since quick and computationally cheap calculations are enabled, which are more easily and efficiently included in the electronic boards that ultimately apply the optimal control strategy in physical systems.

A further novelty of this paper is to apply the pseudospectral approximation framework to extensively discuss the dynamic response of the VEH for different choices of the time-varying damping profile, considering virtually any combination of superharmonics, balancing pros and cons, and quantifying the consequent margins in power extraction, while measuring velocity and force states (usually proxy for costs or imposing design restrictions). In particular, unconstrained active control is firstly considered, defining the intrinsic capabilities of each damping profile, and setting the best benchmark. Secondly, passivity constraints are introduced, in order to quantify the loss in power conversion ability, bargained for a cheaper PTO.

The reminder of the paper is organized as follows: Sect. 1.1 presents some preliminary notation, used in Sect. 2 to univocally define the problem in general terms, and in Sect. 3 to frame the pseudospectral-based approach to determine algebraically the steady-state response. Section 4 presents a numerical case study to enable practical discussion, whose results are presented in Sect. 5. Some closing remarks are provided in Sect. 6.

1.1. Notation and Preliminaries

Standard notation is considered throughout this study. $\mathbb{R}^+$ ($\mathbb{R}^-$) denotes the set of non-negative (non-positive) real numbers. $\mathbb{C}^0$ denotes the set of pure-imaginary complex numbers. The symbol 0 stands for any zero element, dimensioned according to the context. The notation $\mathbb{N}_q$ indicates

[1]Though, typically, pseudospectral techniques are used to compute numerical solutions of partial differential equations, applications of pseudospectral methods to simulation/control of systems defined by ordinary differential equations are often considered within the system dynamics and control community (see, for instance, [28, 30, 31]).

the set of all positive natural numbers up to q, *i.e.* $\mathbb{N}_q = \{1, 2, \ldots, q\}$. The symbol $\mathbb{I}_n$ denotes the identity matrix of order n. The spectrum of a matrix $A \in \mathbb{R}^{n\times n}$, *i.e.* the set of its eigenvalues, is denoted by $\lambda(A)$. The superscript $^\intercal$ denotes the transposition operator. The symbol $\bigoplus$ denotes the direct sum of n matrices, *i.e.* $\bigoplus_{i=1}^{n} A_i = \text{diag}(A_1, A_2, \ldots, A_n)$. The generalised *Dirac-δ* function, shifted by $t_j \in \mathbb{R}^+$, is denoted as $\delta_{t_j} = \delta(t - t_j)$. The *Kronecker product* between two matrices $M_1 \in \mathbb{R}^{n\times m}$ and $M_2 \in \mathbb{R}^{p\times q}$ is denoted by $M_1 \otimes M_2 \in \mathbb{R}^{np\times mq}$. The Hilbert space of square-integrable functions is denoted as $L^2(\Xi) = \{f : \Xi \to \mathbb{R} \mid \int_\Xi |f(\tau)|^2 d\tau < +\infty\}$, where $\Xi \subset \mathbb{R}$ is closed. Finally, the inner-product between two functions $\{f, g\} \subset L^2(\Xi)$ is denoted (and computed) as $\langle f, g\rangle = \int_\Xi f(\tau)g(\tau)d\tau$.

In the remainder of this section, the formal definition of an important operator is presented.

Definition 1 (Vec operator)**.** [32] Given a matrix $P = [p_1, p_2, \ldots, p_m] \in \mathbb{R}^{n\times m}$, where $p_j \in \mathbb{R}^n$, $j \in \mathbb{N}_m$, the vector valued operator *vec* is defined as

$$\text{vec}\{P\} \triangleq \begin{bmatrix} p_1 \\ p_2 \\ \vdots \\ p_m \end{bmatrix} \in \mathbb{R}^{nm}. \tag{1}$$

Finally, we recall a useful set of properties associated with both operators defined above.

Property 1. [32] Let P_1 and P_2, with $P_1 \in \mathbb{R}^{n\times n}$ and $P_2 \in \mathbb{R}^{k\times k}$. Then

$$\lambda(P_1 \hat{\oplus} P_2) = \lambda(P_1) + \lambda(P_2), \tag{2}$$

where the operator "+" refers, in this context, to the Minkowski sum of two sets.

Property 2. [32] Let $P_3 \in \mathbb{R}^{n\times m}$ and $P_4 \in \mathbb{R}^{m\times q}$. Then

$$\text{vec}\{P_3P_4\} = (\mathbb{I}_q \otimes P_3)\text{vec}\{P_4\} = (P_4^\intercal \otimes \mathbb{I}_n)\text{vec}\{P_3\}. \tag{3}$$

2. Problem definition

2.1. System model

The electromechanical energy harvester is modelled as a single-degree of freedom (SDOF) system, as schematically represented in Fig. 1, composed of a mass $m \in \mathbb{R}^+$, attached to a vibrating base by means of a suspension stiffness $k \in \mathbb{R}^+$ and a PTO unit for energy conversion. It is assumed that the PTO force is proportional to the relative velocity between the mass and the base, with a total PTO coefficient defined in terms of a time-varying mapping $c_{\text{PTO}} : \mathbb{R}^+ \to \mathbb{R}$, $c_{\text{PTO}}(t) = b^0_{\text{PTO}} + b_{\text{PTO}}(t)$, where $b^0_{\text{PTO}} \in \mathbb{R}$ represents a predefined mean PTO damping. Internal dissipations are notionally modelled via a linear damper, with constant coefficient $c_d \in \mathbb{R}^+$.

The equation of motion of the SDOF system follows directly from Newton's second law of motion[2], *i.e.*

$$m\ddot{x} + c(t)\,(\dot{x} - \dot{y}) + k\,(x - y) = 0, \tag{4}$$

[2]From now on, the dependence on t is omitted when it is clear from the context.

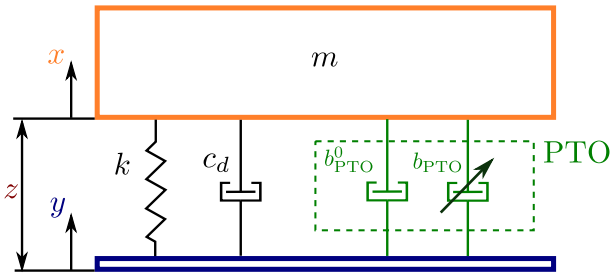

Figure 1: Scheme of the single-degree of freedom vibration energy harvester.

with $x : \mathbb{R}^+ \to \mathbb{R}$, $t \mapsto x(t)$, being the displacement of the mass, $y : \mathbb{R}^+ \to \mathbb{R}$, $t \mapsto y(t)$, the prescribed displacement of the base, and $c(t) = c_d + c_{\mathrm{PTO}}(t)$ the *total* time-varying damping. Defining the relative displacement as $z = x - y$, and assuming a harmonic (cosine) monochromatic base excitation at angular frequency ω, equation (4) can be written as

$$m\ddot{z} + c_d\dot{z} + (b^0_{\mathrm{PTO}} + b_{\mathrm{PTO}}(t))\dot{z} + kz = f_e(t), \tag{5}$$

where $f_e(t) = m\omega^2 y_0 \cos(\omega t) = F_e \cos(\omega t)$, $F_e \in \mathbb{R}$, is the so-called *excitation force*, and y_0 is the amplitude of base displacement. From now on, the *fundamental frequency* ω_0 is set equal to the excitation frequency ω, while its associated period $T_0 = 2\pi/\omega_0$ is called *fundamental period*. Fundamental period and frequency are used in the formulation of the pseudospectral-based approach, in Sect. 3, and in the definition of the PTO damping, in Sect. 2.3.

2.2. Optimal control problem

The objective treated in this paper boils down to find an appropriate design for the time-varying mapping b_{PTO} such that the energy absorbed by the harvester is *maximized*. In other words, this design entails an *energy-maximization* criterion, where the objective is to maximise the absorbed energy from the corresponding base excitation, over a finite time interval[3] $\Xi = [0, T] \subset \mathbb{R}^+$. To be precise, the useful energy absorbed from the excitation input is converted in the PTO system, and can be directly computed as the time integral of converted (instantaneous) power: Let $u = (b^0_{\mathrm{PTO}} + b_{\mathrm{PTO}}(t))\dot{z}$ be defined as the *control force* (*i.e.* PTO input); Then, this energy-maximizing design procedure can be cast as an optimal control problem (OCP), with *objective function* $\mathcal{J}$ defined as

$$\mathcal{J}(b_{\mathrm{PTO}}) = \frac{1}{T}\int_{\Xi} (b^0_{\mathrm{PTO}} + b_{\mathrm{PTO}}(t))\dot{z}^2(\tau)d\tau, \tag{6}$$

With the definition of the control objective function in (6) (*i.e.* the mapping $\mathcal{J}$), and the dynamics of the energy harvester in (5), the energy-maximizing OCP can be formally posed as follows.

Problem 1 (Energy-maximizing OCP)**.** Find an optimal control damping $b^{\mathrm{opt}}_{\mathrm{PTO}} : \Xi \to \mathbb{R}$ such that

$$\begin{aligned} b^{\mathrm{opt}}_{\mathrm{PTO}} &= \arg\max_{b_{\mathrm{PTO}}} \ \mathcal{J}(b_{\mathrm{PTO}}), \\ &\text{subject to:} \\ &\text{Energy harvester dynamics (5).} \end{aligned} \tag{7}$$

[3]Note that there is no loss of generality in setting the initial time to 0.

2.3. On the selection of b_{PTO}

Since the external excitation is harmonic, it is sensible to let b_{PTO} have a harmonic form. Note that, though not an absolute requirement nor condition for optimality, this is in line with previous work performed in [25] and [21]. In the light of this, from now on, we let the time-varying damping b_{PTO} to be defined as

$$b_{\mathrm{PTO}}(t) = \sum_{p=1}^{N} \alpha_p^b \cos(p\omega_0 t) + \beta_p^b \sin(p\omega_0 t), \tag{8}$$

with $N \in \mathbb{N}$, and where $\{\alpha_p^b, \beta_p^b\}_{p=1}^N \subset \mathbb{R}$. In other words, b_{PTO} is defined as a T_0-periodic function, composed of a finite number of harmonics of the input fundamental frequency ω_0. Note that, clearly, $b_{\mathrm{PTO}} \in L^2(\Xi_0)$, with $\Xi_0 = [0, T_0]$. In preparation for the upcoming results, Equation (8) is written in more convenient and compact form, namely

$$b_{\mathrm{PTO}}(t) = B_{\mathrm{PTO}}\xi_N(t), \tag{9}$$

where $\{B_{\mathrm{PTO}}^{\intercal}, \xi_N(t)\} \subset \mathbb{R}^{2N}$, with $B_{\mathrm{PTO}} = [\alpha_1^b\, \beta_1^b \ldots \alpha_N^b\, \beta_N^b]$ and $\xi_N(t) = [\cos(\omega_0 t)\ \sin(\omega_0 t) \ldots \cos(N\omega_0 t)\ \sin(N\omega_0 t)]^{\intercal}$.

Remark 1. The instantaneous power for the selected control force $u = (b_{\mathrm{PTO}}^0 + b_{\mathrm{PTO}}(t))\dot{x}$, which is effectively the term to be integrated in (6), can be simply computed as $P = u\dot{x} = (b_{\mathrm{PTO}}^0 + b_{\mathrm{PTO}}(t))\dot{x}^2$. From the equation of P, it is straightforward to conclude that the instantaneous power will be negative if and only if $b_{\mathrm{PTO}}^0 + b_{\mathrm{PTO}}(t) < 0$, for any $t \in \Xi_0$. Note that, given that b_{PTO} is a zero-mean function (see equation (8)), this change in sign happens if any negative peak of b_{PTO} is effectively larger (in magnitude) than the constant value b_{PTO}^0. When the instantaneous power P is negative, there is a power flow from the PTO to the energy harvesting device. If this happens, the controller is said to be an *active controller*.

3. A pseudospectral-based approach

We begin by re-writing the dynamical equation (5) in a more suitable form for the approach presented in this section. In particular, let $\varphi(t) = [\varphi_1(t), \varphi_2(t)]^{\intercal} = [z(t),\ \dot{z}(t)]^{\intercal} \in \mathbb{R}^2$ be the state-vector associated with equation (5). Then, the dynamical relation (5) can be written in terms of a time-varying state-space system as

$$\begin{aligned} \dot{\varphi} &= A\varphi + Bf_e - B(b_{\mathrm{PTO}}^0 + b_{\mathrm{PTO}}(t))y, \\ y &= C\varphi = \dot{z}, \end{aligned} \tag{10}$$

where the triple of matrices (A, B, C) are given by

$$A = \begin{bmatrix} 0 & 1 \\ -k/m & -c_d/m \end{bmatrix}, B = \begin{bmatrix} 0 \\ 1/m \end{bmatrix}, C^{\intercal} = \begin{bmatrix} 0 \\ 1 \end{bmatrix}, \tag{11}$$

Note that velocity $\dot{z}$ is considered to be the output of system (10) given its inherent connection to the objective function defined in equation (6) (and hence the associated energy-maximising

OCP of Problem 1). We note that this is done *without any loss of generality*, and that either displacement or acceleration can be equally considered within the subsequent propositions, by performing an analogous analysis. The following standing assumption is now presented, which is required to prove existence of T_0-periodic solutions for system (10).

Assumption 1. System is (10) is uniformly exponentially stable.

Remark 2. Assumption 1 guarantees that there exists a set of constants $\{\gamma_1, \gamma_2\} \subset \mathbb{R}^+$ such that, for any t_0 and $\varphi(t_0)$, the solution of (10) with $f_e = 0$ satisfies the relation $\|\varphi(t)\| \leq \gamma_1 e^{-\gamma_2(t-t_0)}$, for every $t \geq t_0$ (see, for instance, [33]). This directly implies bounded-input bounded-output (BIBO) (*i.e.* input-output) stability. Note that the requirement posed in Assumption 1 is consistent with the underlying physics of the energy harvesting process.

The following proposition is now presented, which guarantees existence of T_0-periodic solutions for system (10) driven by the excitation input f_e, providing a fundamental stepping-stone for the proposed optimal control procedure.

Proposition 1. *Let $\varphi^{ss} : \mathbb{R}^+ \to \mathbb{R}^2$, $t \mapsto \varphi^{ss}(t)$, be the steady-state solution of system* (10) *driven by the excitation force f_e. Suppose b_{PTO} is as defined in* (8)*, and Assumption 1 holds. Then, the mapping φ^{ss} is T_0-periodic.*

Proof. See Appendix A for the proof. □

Remark 3. The result posed in Proposition 1 allows each mapping φ_k^{ss}, $k \in \mathbb{N}_2$, to be uniquely expressed in terms of the standard canonical basis of $L^2(\Xi_0)$, *i.e.*

$$\varphi_k^{ss}(t) = \left(\sum_{p=1}^{M} \alpha_p^{\varphi_k} \cos(p\omega_0 t) + \beta_p^{\varphi_k} \sin(p\omega_0 t) \right) + \epsilon_k(t) = \bar{\Phi}_k \xi_M(t) + \epsilon_k(t), \tag{12}$$

with $M \geq N$, and where the vector elements $\{\bar{\Phi}_k^\intercal, \xi_M(t)\} \subset \mathbb{R}^{2M}$ are defined such that $\bar{\Phi}_k = [\alpha_1^{\varphi_k}\ \beta_1^{\varphi_k}\ \dots\ \alpha_M^{\varphi_k}\ \beta_M^{\varphi_k}]$ and $\xi_M(t) = [\cos(\omega_0 t)\ \sin(\omega_0 t)\ \dots \cos(M\omega_0 t)\ \sin(M\omega_0 t)]^\intercal$. The mapping ϵ_k, herein termed as 'reminder', is defined as

$$\epsilon_k(t) = \sum_{q=M+1}^{\infty} \alpha_q^{\varphi_k} \cos(q\omega_0 t) + \beta_q^{\varphi_k} \sin(q\omega_0 t). \tag{13}$$

Note that the expansion presented in Remark 3 allows the steady-state response mapping φ^{ss} to be compactly expressed as

$$\varphi^{ss} = \begin{bmatrix} \bar{\Phi}_1 \\ \bar{\Phi}_2 \end{bmatrix} \xi_M + \begin{bmatrix} \epsilon_1 \\ \epsilon_2 \end{bmatrix} = \bar{\Phi}\xi_M + E, \tag{14}$$

where, from now on, the term $E : \mathbb{R}^{2M} \to \mathbb{R}^2$ is called the *truncation* error.

If the truncation error E is 'ignored', the mapping φ^{ss} can be effectively approximated as $\varphi^{ss} \approx \bar{\Phi}\xi_M$, *i.e.* by its expansion on the $2M$-dimensional set spanned by the entries of ξ_M. This motivates the following key definition.

Definition 2. The function $\varphi_M^{ss} : \mathbb{R}^+ \to \mathbb{R}^2$, where $\varphi_M^{ss} = \bar{\Phi}\xi_M$, is called the $2M$-dimensional approximation of the steady-state response of system (10) driven by f_e.

Following the formal definition of steady-state response approximation posed in Definition 2, and in preparation for the upcoming results, a set of fundamental remarks are now introduced.

Remark 4. The time-derivative of the approximated steady-state response mapping φ_M^{ss} can be readily computed as

$$\dot{\varphi}_M^{ss} = \bar{\Phi}\dot{\xi}_M = \bar{\Phi}S\xi_M, \tag{15}$$

where the block-diagonal matrix $S \in \mathbb{R}^{2M\times 2M}$ is defined as

$$S = \bigoplus_{p=1}^{2M} \begin{bmatrix} 0 & p\omega_0 \\ -p\omega_0 & 0 \end{bmatrix}. \tag{16}$$

Remark 5. Given that the relation $\xi_M = [\xi_N^\intercal \, \xi_{M-N}^\intercal]^\intercal$, where $\xi_{M-N}^\intercal(t) = [\cos((N+1)\omega_0 t) \, \sin(\omega_0 t) \, \ldots \cos(M\omega_0 t) \, \sin(M\omega_0 t)]^\intercal$, holds, it is straightforward to note that both input f_e, and time-varying damping b_{PTO}, can be written in terms of ξ_M by the use of an appropriate inclusion mapping, *i.e.* by completing with zeros accordingly. To be precise:

$$\begin{aligned} f_e &= F_e \cos(\omega_0 t) = [F_e \; 0]\xi_M = \bar{F}_e\xi_M, && \textit{i.e.} \text{ the map } \mathbb{R}^{1\times n} \hookrightarrow \mathbb{R}^{1\times 2M}, F_e \mapsto \bar{F}_e, \\ b_{\text{PTO}} &= B_{\text{PTO}}\, \xi_N = [B_{\text{PTO}}\, 0]\xi_N = \bar{B}_{\text{PTO}}\xi_M && \textit{i.e.} \text{ the map } \mathbb{R}^{1\times 2N} \hookrightarrow \mathbb{R}^{1\times 2M}, B_{\text{PTO}} \mapsto \bar{B}_{\text{PTO}}. \end{aligned} \tag{17}$$

Aiming to propose a method to compute $\bar{\Phi}$, for every admissible $\bar{B}_{\text{PTO}}$, a strategy based on the family of mean weighted residual methods [28, 34] is proposed. In particular, the following *residual* mapping $\mathcal{R} : \mathbb{R}^{2\times 2M} \times \mathbb{R}^{1\times 2M} \times \mathbb{R}^{2M} \to \mathbb{R}^2$ is defined as

$$\mathcal{R}(\bar{\Phi}, \bar{B}_{\text{PTO}}, \xi_M(t)) := \left(\bar{\Phi}S - A\bar{\Phi} - B\bar{F}_e\right)\xi_M(t) + B(C\bar{\Phi}\xi_M(t))(b_{\text{PTO}}^0 + \bar{B}_{\text{PTO}}\xi_M(t))^\intercal, \tag{18}$$

which directly arises from 'replacing' φ with φ_M^{ss} in equation (10), and considering f_e and b_{PTO} as in (17). Since (18) directly depends on t, a *pseudospectral* (or *collocation*) approach [35, Chapter 4] is considered to map the residual equation onto a finite-dimensional space. In other words, equation (18) is forced to be exactly zero at a finite set of *collocation* points:

$$\langle \mathcal{R}(\bar{\Phi}, \bar{B}_{\text{PTO}}, \xi_M), \delta_{t_j} \rangle = 0, \tag{19}$$

for every $j \in \mathbb{N}_{2M}$, with $\mathcal{T}_\delta = \{t_j\}_{j=1}^{2M} \subset \Xi_0$ a set of uniformly-distributed time instants. This gives origin to a system of algebraic equations, which is explicitly written in compact form as a result of the following proposition.

Remark 6. The selection of a pseudospectral approach for the projection of the residual equation, *i.e.* equation (19), is merely motivated by the simplicity behind the collocation nature of the method, and the analytical structure of the approximated solution (which is exploited in Proposition 2). Nonetheless, we do note that other techniques from the general family of weighted residual methods can be alternatively considered (see [34]).

Proposition 2. *The system of algebraic equations* (19) *can be equivalently written in matrix form as*

$$\bar{\Phi}S - A\bar{\Phi} - B\bar{F}_e + BC\bar{\Phi}\mathcal{M}(\bar{B}_{PTO})\Omega^{-1} = 0, \tag{20}$$

where the matrices $\{\mathcal{M}(\bar{B}_{PTO}), \Omega\} \subset \mathbb{R}^{2M\times 2M}$ *are defined as*

$$\begin{aligned}\Omega &= \begin{bmatrix}\xi(t_1) & \dots & \xi(t_{2M})\end{bmatrix},\\ \mathcal{M}(\bar{B}_{PTO}) &= b^0_{PTO}\Omega + \begin{bmatrix}\xi(t_1)\xi(t_1)^\intercal \bar{B}^\intercal_{PTO} & \dots & \xi(t_{2M})\xi(t_{2M})^\intercal \bar{B}^\intercal_{PTO}\end{bmatrix}.\end{aligned} \tag{21}$$

Proof. See Appendix B for the proof. □

The result of Proposition 2 allows the compute the $2M$-dimensional approximation of the steady-state response of system (10) in terms of the set of algebraic equations (20), which can be solved by means of state-of-the-art root-finding algorithms (see, for instance, [36]). Nonetheless, it is important to derive explicit conditions for the existence of unique solutions to equation (20). This is explicitly addressed in the following paragraphs.

Assumption 2. The spectra of $A+BC$ and $S+\mathcal{M}(\bar{B}_{\mathrm{PTO}})$ are disjoint, *i.e.* $\lambda(S+\mathcal{M}(\bar{B}_{\mathrm{PTO}})\Omega^{-1})\cap \lambda(A+BC)=\emptyset$, for every admissible $\bar{B}_{\mathrm{PTO}}$.

Proposition 3. *Suppose Assumption 2 holds. Then, the system of algebraic equations* (20) *admits a unique solution.*

Proof. See Appendix C for the proof. □

Remark 7. Though potentially difficult to verify analytically, numerical experience suggests that, for any physically meaningful values of the parameters involved in the equation of motion (10), Assumption 2 is always consistent.

3.1. Pseudospectral-based OCP

The results presented up until this point can be effectively used to approximate the energy-maximising optimal control problem presented in Problem 1. In the following, we provide a definition of the so-called *approximated energy-maximizing* OCP, in terms of the approximated steady-state response mapping φ^{ss}_M, presented in Definition 2, together with the results posed in Propositions 2 and 3.

Problem 2 (Approximated energy-maximizing OCP)**.** Let b_{PTO} be defined as in (8). Suppose Assumptions 1 and 2 hold. Find the optimal control damping $b^{\mathrm{opt}}_{\mathrm{PTO}} = \bar{B}^{\mathrm{opt}}_{\mathrm{PTO}}\xi_M$ such that

$$\begin{aligned}\bar{B}^{\mathrm{opt}}_{\mathrm{PTO}} = \arg\max_{\bar{B}^\intercal_{\mathrm{PTO}}\in\mathbb{R}^{2M}} \frac{1}{T_0}\int_{\Xi_0} C\bar{\Phi}\xi_M(\tau)\left(b^0_{\mathrm{PTO}} + \bar{B}_{\mathrm{PTO}}\xi_M(\tau)\right)\left(C\bar{\Phi}\xi_M(\tau)\right)^\intercal d\tau,\\ \text{subject to:}\\ \mathcal{W}(\bar{B}_{\mathrm{PTO}})\,\mathrm{vec}\{\bar{\Phi}\} - (\mathbb{I}_{2M}\otimes(-B))\mathrm{vec}\{\bar{F}_e\} = 0.\end{aligned} \tag{22}$$

Remark 8. The main idea behind Problem 2 relies on substituting the integro-differential (equality) constraint in the target energy-maximizing Problem 1, corresponding with the energy harvester dynamics (10), by the *algebraic* equation derived via the proposed framework (C.2). In other words, the approximated OCP posed in Problem 2 explicitly utilises an approximation of the steady-state (output) behaviour of system (10), parametrised in terms of $\bar{\Phi}$, to solve for the corresponding optimal control damping $b^{\mathrm{opt}}_{\mathrm{PTO}}$. Note that, given the T_0-periodicity of the associated steady-state response mapping, it is sufficient to integrate the objective function over a single period, *i.e.* over the set Ξ_0.

The OCP posed in Problem 2 can be further simplified, by virtue of the results presented throughout this section. In particular, the following proposition shows that the presence of the equality constraint in (22) can be avoided altogether, and a finite-dimensional unconstrained nonlinear program can be constructed for the computation of an optimal PTO damping, which solely depends upon $\bar{B}_{\mathrm{PTO}}$.

Proposition 4 (Pseudospectral-based nonlinear program)**.** *Let b_{PTO} be defined as in* (8)*. Suppose Assumptions 1 and 2 hold. Then, the solution of the approximated energy-maximizing OCP, posed in Problem 2, can be computed as $b_{PTO}^{opt} = \bar{B}_{PTO}^{opt}\xi_M$, where $\bar{B}_{PTO}^{\mathrm{opt}}$ is the solution of the finite-dimensional nonlinear program*

$$\bar{B}_{PTO}^{opt} = \arg \max_{\bar{B}_{PTO}^{\intercal} \in \mathbb{R}^{2M}} \frac{1}{T_0} \left(\bar{F}_e \bar{\mathcal{W}}(\bar{B}_{PTO}) \otimes \bar{F}_e \bar{\mathcal{W}}(\bar{B}_{PTO}) \right) \left[b_{PTO}^0 \mathcal{X}_1 + \mathcal{X}_2 \bar{B}_{PTO}^{\intercal} \right], \tag{23}$$

where the mapping $\bar{\mathcal{W}} : \mathbb{R}^{1\times 2M} \to \mathbb{R}^{2M\times 2M}$ is defined as

$$\bar{\mathcal{W}}(\bar{B}_{PTO}) = \left[(\mathbb{I}_{2M} \otimes C) \mathcal{W}(\bar{B}_{PTO})^{-1} (\mathbb{I}_{2M} \otimes (-B)) \right]^{\intercal}, \tag{24}$$

and the matrices $\mathcal{X}_1 \in \mathbb{R}^{M^2}$, $\mathcal{X}_2 \in \mathbb{R}^{M^2\times M}$, are given by the following expressions:

$$\mathcal{X}_1 = \int_{\Xi_0} (\xi_M(\tau) \otimes \xi_M(\tau))\, d\tau, \quad \mathcal{M}_2 = \int_{\Xi_0} (\xi_M(\tau) \xi_M(\tau)^{\intercal} \otimes \xi_M(t))\, d\tau. \tag{25}$$

Proof. See Appendix D for the proof. □

Remark 9. Note that the integral operations defined in the set of matrices $\{\mathcal{X}_1, \mathcal{X}_2\}$ can be readily computed 'offline', since their evaluation *only* depends upon the definition of ξ_M and T_0, which are pre-defined by the user.

Remark 10. The finite-dimensional nonlinear program derived in Proposition 4 can be solved using computationally efficient state-of-the-art nonlinear optimization routines, such as those belonging to the family of interior point methods (see, for instance, [37]). In particular, for the results presented in Section 4, the IPM proposed in [38] is considered, which is implemented in MATLAB® via the native function *fmincon*.

4. Case study - numerical analysis

A numerical example is herein defined in order to analyse the system and provide a deep insight on the performance of the VEH. Since the model is linear, despite time-variant, results can be extrapolated to different sizes and scales with virtually no loss of fidelity. Therefore, the system parameters, tabulated in Table 1, are chosen so that the natural frequency (ω_n) of the linear system is equal to 1 Hz. A relatively small, although not negligible, internal damping coefficient is included, realizing a damping ratio (ζ) of 2%; in fact, consistent with indications provided in [21], when parasitic dissipations are low, active control strategies are likely to have an edge over semi-active approaches. The linear time-invariant (LTI) system, associated to the model in (5) with parameters in Table 1 when b_{PTO} is zero, is represented in the Bode plot of Fig. 2.

A constant mean PTO damping coefficient has been assumed for all control conditions, since the focus of the current investigation is on the time-varying components. Therefore, an optimization or

Table 1: System parameters of vibration energy harvester in the numerical case study.

Parameter	**Symbol**	**Unit**	**Value**
Mass	m	[kg]	2
Spring	k	[N/m]	$8\pi^2$
Undamped natural frequency	$\omega_n = \sqrt{k/m}$	[rad/s]	2π
Base amplitude displacement	y_0	[m]	0.01
Internal damping ratio	$\zeta_d = \frac{c_d}{2\sqrt{km}}$	[-]	2%
Internal damping coefficient	c_d	[Ns/m]	0.5027
Mean PTO damping ratio	$\zeta^0_{\mathrm{PTO}} = 0.5\zeta_d$	[-]	1%
Mean PTO damping coefficient	b^0_{PTO}	[Ns/m]	0.2513

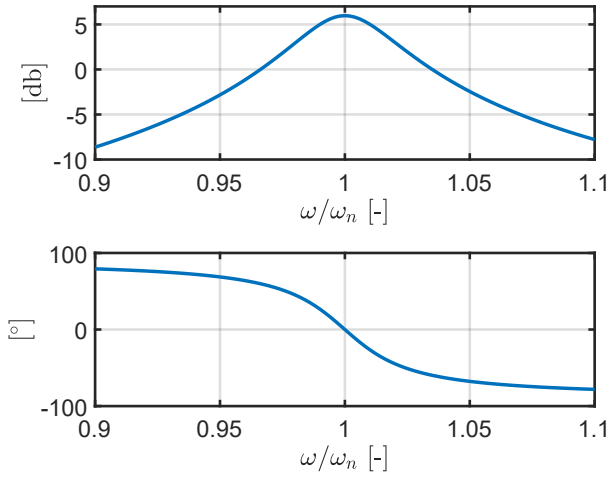

Figure 2: Bode plot of the associated linear time-invariant system (force-to-velocity).

sensitivity study on variations of b^0_{PTO} lays outside the scope of the present paper. On the contrary, in order to clearly understand and quantify the benefits of harmonic variations of b_{PTO}, different combinations of sine and cosine of various orders are forced in the optimization algorithm; in this way, it is possible to discriminate which terms are dominantly responsible for the performance enhancement, and in which frequency range. Such an analysis is also crucial to discern inherent limitations of different control laws, which may pass unperceived if a single functional term is considered [21].

Table 2 shows schematically the most relevant cases considered, representing the absence of a term with an empty circle, and the presence with a full circle. Let us remind, as defined in (8), that α and β refers respectively to cosine and sine terms, while the subscript refers to the order. The case naming presents subscripts referring to the orders included (number), cosine ($_c$) and sine ($_s$). Following such a naming convention, N_0 stands for no harmonic variations of c_{PTO}, *i.e.* a simple constant coefficient, providing the *worst-performance benchmark*. N_{1c} presents a b_{PTO} varying with just a cosine term of the first order, *i.e.* at the same frequency of the excitation force and always in phase. At resonance, as shown in Fig. 2, the velocity is in phase with the excitation force, hence also with b_{PTO} for N_{1c}. However, the velocity tends to go in phase quadrature moving away from

resonance, as fast as small is the total damping ratio of the system; it follows that the variations of b_{PTO} for N_{1c} move out of phase with the velocity as the frequency diverges from resonance. Conversely, N_{1cs}, has the structure to realize arbitrary phase differences with respect to f_e, hence the velocity, thanks to appropriate combinations of sine and cosine terms. Therefore, comparing N_{1c} with N_{1cs} it is possible to infer if phase differences of time-variations of the first order of b_{PTO} are beneficial. A similar interplay is realized in N_{2c} and N_{2cs}: in both such cases, time-variations of b_{PTO} are purely of twice the frequency of f_e; however, the phase in N_{2c} is locked to be the same of the external input, while in N_{2cs} there is the freedom of adjusting the phase optimally. Finally, N_{12cs} potentially combines all terms of first and second orders, granting the optimization algorithm the highest tuning freedom within the set in Table 2, hence providing the *best-performance benchmark*. It is important to note that higher orders have been considered (N_{123cs} and N_{1234cs}), but the algorithm numerically optimizes coefficients of the higher harmonics to zero, highlighting that including one odd harmonic (first order) and one even harmonic (second order) is sufficient to insert beneficial additional dynamics, while further harmonics become redundant.

In Sect. 5, results are presented, considering at first representative time traces, in Sect. 5.1, while in Sect. 5.2 further discussion of synthetic results is provided, including optimal damping coefficients and power extraction for all cases shown in Table 2.

Table 2: Control laws summary, where α and β refers respectively to coefficients of cosine and sine terms, while the subscript refers to the order: an empty circle means the absence of a term whereas a full circle represents the presence. The subscripts of the control law naming code refer to the order (number) and the presence of the cosine ($_c$) or sine ($_s$).

Control law	α_1	β_1	α_2	β_2
N_0	○	○	○	○
N_{1c}	●	○	○	○
N_{1cs}	●	●	○	○
N_{2c}	○	○	●	○
N_{2cs}	○	○	●	●
N_{12cs}	●	●	●	●

5. Results

5.1. Time traces

Numerical results are produced using the mathematical method described in Sect. 3, enabling to promptly return the steady-state solution via simple algebraic calculations. The effectiveness of the underlying theory and correctness of the implementation is numerically verified by comparing the prediction of the pseudospectral approach, in terms of simulation, to the time trace computed via a standard time-advancing scheme (Runge-Kutta). In particular, we show in the following that the approximation of the steady-state response of the energy harvester, posed in Definition 2 and computed via Proposition 2, is effectively both correct and consistent. From now on, the number of functions used to approximate the steady-state response mapping, *i.e.* M, is set to $M = 10$, which is sufficiently large to characterise the steady-state response with a high degree of accuracy. Figure 3 shows an example of the successful comparison, using the N_{2c} control law at ω/ω_n of 1.05, simulating up to 50 fundamental periods. The steady-state is correctly described, regardless

of the potential overshooting of the transient, as in Fig. 3. This is particularly beneficial in cases with low internal damping, where transients may last several fundamental periods, making the numerical integration scheme especially time consuming, in principle also requiring convergence checks. Conversely, the proposed pseudospectral method algebraically computes the steady-state, regardless of the transient path.

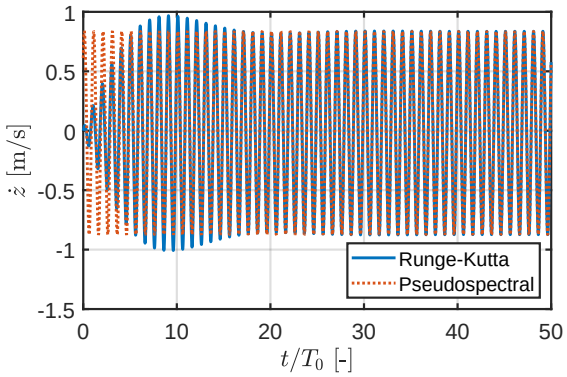

Figure 3: Numerical validation: comparison of time trace computed with time-advancing scheme (Runge-Kutta) and the steady-state computed with the pseudospectral approach, for the case N_{2c} at $\omega/\omega_n = 1.05$.

In order to increase the understanding on how each control law influences the system dynamics in order to maximise the power capture, highlighting intrinsic limitations, a series of representative time traces over a single steady-state fundamental period are shown, first at resonance, then below (95%) and above (105%), respectively in Figs. 4, 5, and 6. Such plots show the instantaneous power (P), the normalized external force (f_e^*), the normalized velocity ($\dot{z}^*$), and the normalized PTO damping coefficient (c^*_{PTO}), where the normalization is obtained dividing each quantity by its maximum absolute value. Finally, for each control law, the optimal α and β are used. For clarity or representation, N_{1c} and N_{12cs} are omitted, since their time traces and power outputs are similar to N_{1cs} and N_{2cs}, respectively, as further discussed in Sect. 5.2.

Figure 4 shows time traces at resonance. As expected, external force and velocity are in phase for all control laws, as their normalized curves overlap. In fact, one general condition for maximum energy extraction, according to complex-conjugate control (see, for instance, [39]), is phase accordance between excitation force and velocity. At resonance, since the phase match is naturally ensured by the system characteristics, the control force is 'inactive' and the same normalized profiles are found for all control laws. Nevertheless, the c_{PTO} profile changes, from constant in N_0, to first-harmonic in N_{1cs}, to second-harmonic in N_{2c} and N_{2cs}. Since the normalized velocity is the same in all cases, the profiles of instantaneous power change instead, realizing different mean power outputs. In N_{1cs}, the optimal control law parameters require the opposite phase between velocity and damping coefficient ($\alpha_1 < 0, \beta_1 = 0$), realizing a global maximum power output at the trough of $\dot{z}^*$, and a smaller local maximum at the peak of $\dot{z}^*$. Furthermore, the instantaneous power is always positive, hence making the control naturally semi-active. Time traces of N_{2c} and N_{2cs} are exactly equal, highlighting that the sine is not useful to maximise power at resonance, since the appropriate phase difference is spontaneously realized. The second-order harmonic makes c_{PTO} maximum at both the peak and trough of the $\dot{z}$, whereas c_{PTO} is minimum when $\dot{z}$ crosses the zero axis; therefore, the PTO tends to let the system escape the equilibrium position as fast as possible by minimizing the resistance, while applies the maximum

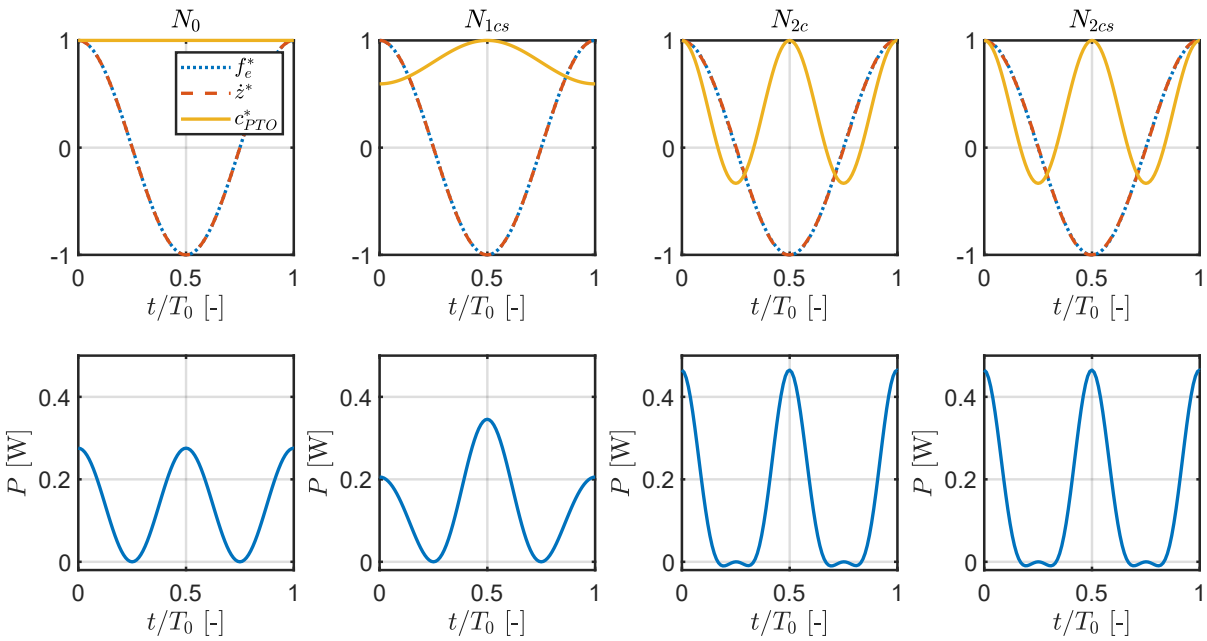

Figure 4: On the top row: normalized external force (f_e^*), normalized velocity ($\dot{z}^*$), and normalized PTO damping coefficient (c_{PTO}^*); on the bottom row: instantaneous power (P). Simulation at $\omega/\omega_n = 1$.

damping as the oscillating mass reaches the furthest positions. The consequent instantaneous power presents global maxima higher than N_{1cs}, and equal at both the peak and trough of $\dot{z}$. In fact, the instantaneous power is proportional to the square of the velocity, so naturally oscillates at twice the frequency of the excitation force; therefore, harmonic variations of c_{PTO} at 2ω best accommodate the time-variations of P.

Figure 4 shows that, at resonance, the best phase difference is naturally ensured by the internal system dynamics, so the sine term of the control law is useless. On the contrary, away from resonance, the velocity would naturally fall behind (for $\omega < \omega_n$) or after (for $\omega > \omega_n$), so the sine term in the control force may play a fundamental role in forcing phase accordance and, consequently, increase power extraction. Figure 5 shows the response at $\omega/\omega_n = 0.95$, confirming the significant phase lag in N_0 and N_{2c}; on the other hand, best matching between f_e^* and $\dot{z}^*$ is realized by N_{2cs}, while N_{1cs} has an acceptable phase accordance but discrepant profiles. The following power output trends are greatly different, with peaks in N_0 between 1 and 3 orders of magnitudes lower than time-varying control laws; however, N_0 is the only naturally non-active control strategy.

Finally, Fig. 6 shows the response at $\omega/\omega_n = 1.05$. Likewise Fig. 5, N_0 and N_{2c} present a phase difference between $\dot{z}$ and f_e, although of different sign, consistent with the Bode plot in Fig. 2. N_{2cs} is again able to correct such a phase lag, driving $\dot{z}$ and f_e in phase and maximising net power extraction, regardless of the negative power flow required to force phase accordance. On the contrary, N_{1cs} basically degenerates into a N_0-like control law, since the alternating components (α_1 nd β_1) are negligible with respect to the mean value (b_{PTO}^0); consequently, the phase lag is not coped with, and power extraction remains low. Comparing Figs. 5 and 6, it is clear that first-order control laws are able to cope with positive phase lags only, *i.e.* at $\omega < \omega_n$; conversely, for negative phase lags, the negative power flow required to achieve phase accordance is greater than the positive extracted power, leading to negative net powers, clearly undesirable.

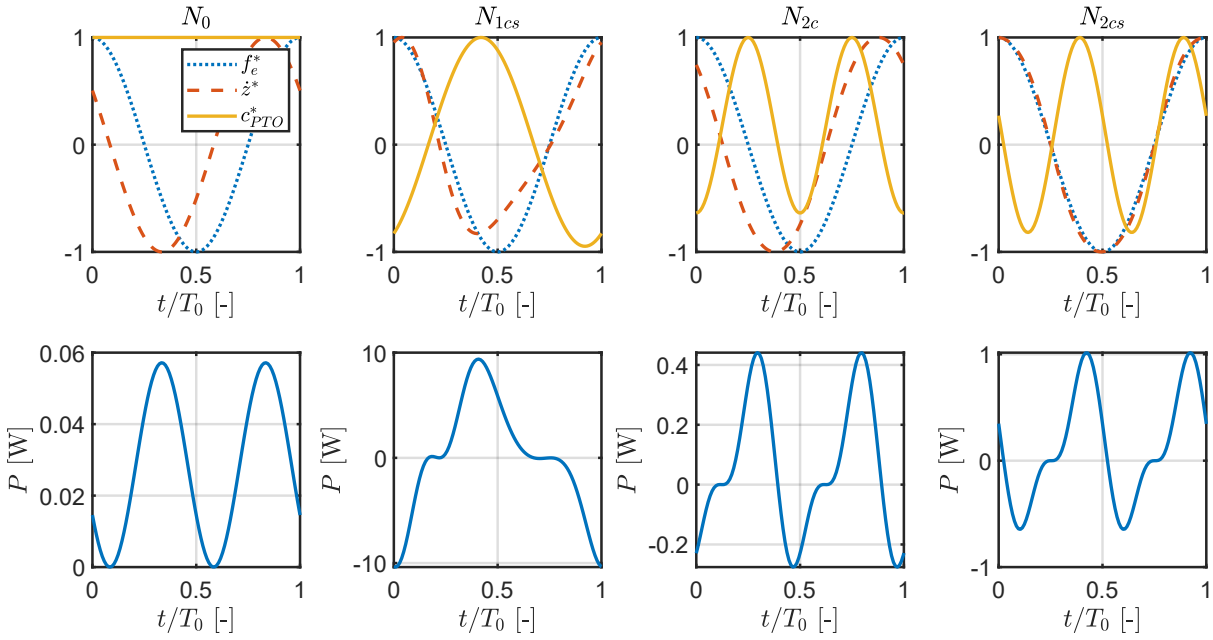

Figure 5: On the top row: normalized external force (f_e^*), normalized velocity ($\dot{z}^*$), and normalized PTO damping coefficient (c_{PTO}^*); on the bottom row: instantaneous power. Simulation at $\omega/\omega_n = 0.95$.

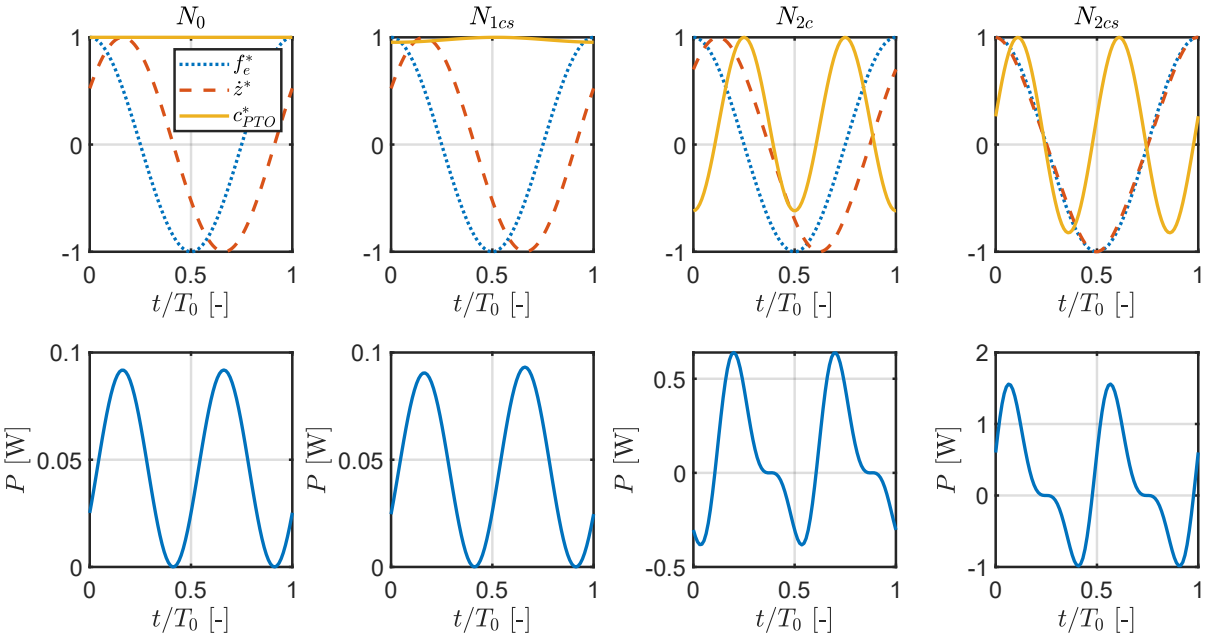

Figure 6: On the top row: normalized external force (f_e^*), normalized velocity ($\dot{z}^*$), and normalized PTO damping coefficient (c_{PTO}^*); on the bottom row: instantaneous power. Simulation at $\omega/\omega_n = 1.05$.

A deeper comparative analysis of first- and second-order control law behaviours is provided in Fig. 7, where the mean net power output ($\overline{P}$) is computed for different settings of the control parameters. In order to ease the sensitivity analysis and the graphical representation, N_{1c} and N_{2c}

are considered, since they both depend on a single amplitude value, respectively α_1 and α_2. Note that similar results may be obtained using both sine and cosine terms, considering the so-called *complex amplitude* ($\sqrt{\alpha^2+\beta^2}$), and selecting the best ratio α/β.

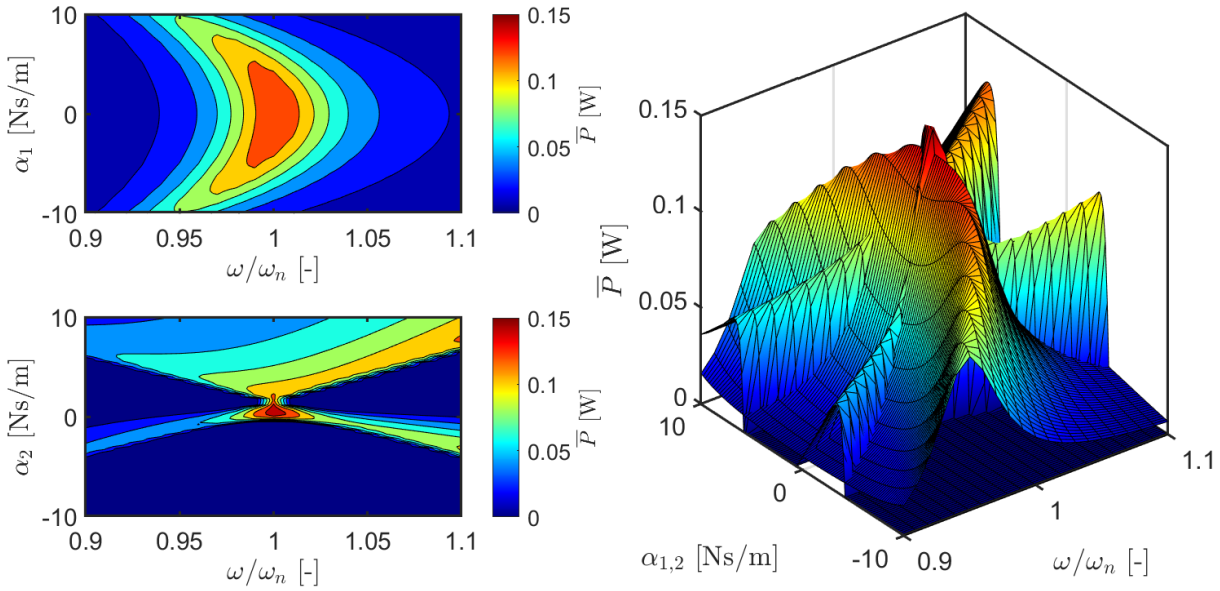

Figure 7: Sensitivity analysis, computing the mean net power ($\overline{P}$) for N_{1c} and N_{2c}, varying α_1 and α_2, respectively. On the left, the top view for N_{1c} (top) and N_{2c} (bottom). On the right, the three-dimensional view for both N_{1c} and N_{2c}, to facilitate the topological cross-comparison.

First-order control law N_{1c} is symmetric with respect to α_1 values, since c_{PTO} variations are in phase with the velocity, and the power is proportional to the velocity squared. Conversely, a bifurcation is found in the frequency direction, with twin peaks for $\omega < \omega_n$ that come together at resonance, and become a single peak for $\omega > \omega_n$. This is consistent with the discussion relative to Figs. 5 and 6. A similar behaviour of the mean net power surface is also found in [40] for vibration mitigation. The second-order control law N_{2c} shows a symmetric bifurcation, with peaks merging only at resonance, while diverging for frequencies both lower and higher. Note that the optimal $\overline{P}$ increases with frequency; in fact, since the base amplitude y_0 is constant, the external excitation force amplitude increases, which is proportional to $y_0\omega^2$. Comparing the three-dimensional views of the power surfaces, it can be appreciated that the power at resonance is comparable. For $\omega < \omega_n$, N_{1c} presents a smooth surface, beneficial for a robust implementation; however, the required α_1 increases rapidly, posing higher demands on the PTO mechanisms, potentially increasing costs. Conversely, N_{2c} realizes higher power outputs, but for a narrow range of α_2, which may cause robustness issues. For $\omega > \omega_n$, the second-order control law greatly outperforms the first-order approach, due to the asymmetry of N_{1c}, but optimal α_2 peaks remain relatively narrow. Finally, note that wrong selection of α_2 may generate negative mean net power (drive energy greater than extracted energy over a cycle): in such instances, $\overline{P}$ has been set to zero, since it is more convenient to not operate.

5.2. Synthetic results

In this section, optimal results for each control law are compared. Figure 8 shows the maximum $\overline{P}$ obtainable with each control profile, on the left, and the ratio with respect to the overall best

performance, on the right. Results in Fig. 8 are consistent with what found in [21], that implemented a N_{2c}-type of control, and with [25], that compared constant- to variable-damping control laws. As expected, N_{12cs} is the golden benchmark, thanks to greater optimization freedom; the maximum extracted power grows proportionally to the incoming energy, *i.e.* $my_0\omega^2$. However, it is interesting to note that including the first order in N_{12cs} is redundant, since the same performance is obtained with N_{2cs}. On the contrary, the second-order sine term is crucial to optimize power extraction away from resonance, greatly expanding the bandwidth. In fact, in the range where the phase lag is about constant and equal to $\pm 90°$ ($\omega < 0.97\omega_n \wedge \omega > 1.03\omega_n$, as shown in the bode plot in Fig. 2), the power extraction efficiency of N_{2c} with respect to N_{2cs} settles down to about 45%. The first-order control laws, both performing similarly with and without the sine terms, show the general asymmetry about ω_n; while there is no performance improvement with respect to N_0 for $\omega > \omega_n$, about a linear enhancement is obtained for lower frequencies where, interestingly, N_{1c} outperforms N_{2c} in the range between of ω between 92% and 99%. However, this comes with high demand of driven power, as shown in Fig. 5. Finally, it is worth noting that power extraction of the LTI system, *i.e.* N_0, follows the amplitude response shown in the Bode plot in Fig. 2.

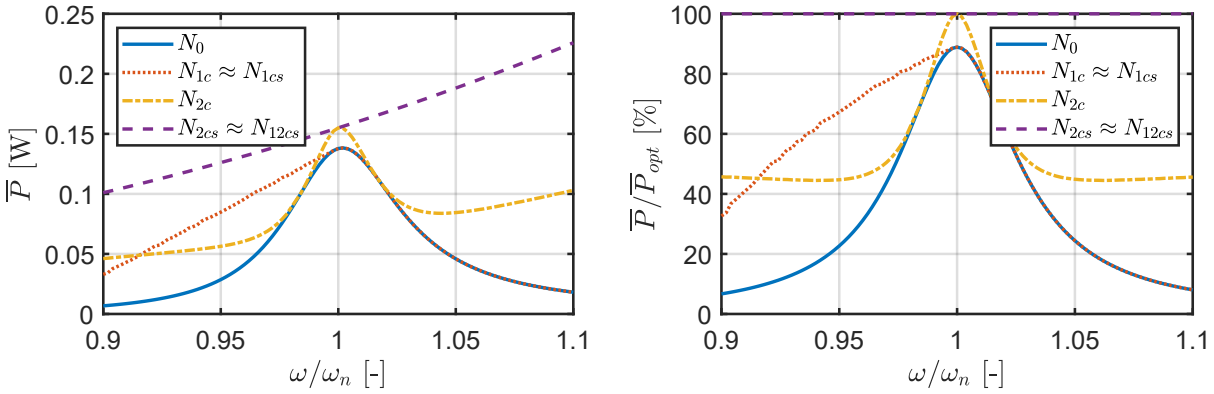

Figure 8: Absolute (left) and relative (right) mean power extraction.

Figure 9 shows the absolute value of the optimized parameters for the considered control laws, at three representative frequencies, *i.e.* 95%, 100%, and 105% of the resonance frequency. The same vertical scale is used for the three graphs, in order to highlight major magnitude differences. In general, the control action is minimal at ω_n, with zero sine components, since the system is naturally in phase and resonance. First-order control laws are powerless to improve the performance for $\omega > \omega_n$, degenerating into N_0; conversely, a relatively very large control action is required in the struggle to improve performance for $\omega < \omega_n$. Note that, passing from N_{1c} to N_{1cs}, part of the spectral energy is transferred from α_1 to β_1, in a ratio such that the complex amplitude remains about the same. The distribution of optimal parameters for the second-order control laws appear to be symmetric with respect to ω_n. Differently from first order, the step from N_{2c} to N_{2cs}, away from ω_n, requires to increase the complex amplitude of the control parameters, *i.e.* α_2 in N_{2c} is lower than $\sqrt{\alpha_2^2 + \beta_2^2}$ in N_{2cs}. Finally, note that the first-order components of N_{12cs} are negligible, remarking that a purely second-order control action is sufficient.

Although power extraction is the prime objective of an energy harvester, techno-economic constraints should play a role in the design and decision process. Physical constraints must be taken into account, such as maximum admissible stroke, available bulk, acceptable velocities to limit wear on components, peak realizable force by the transducer and consequent mechanical stress

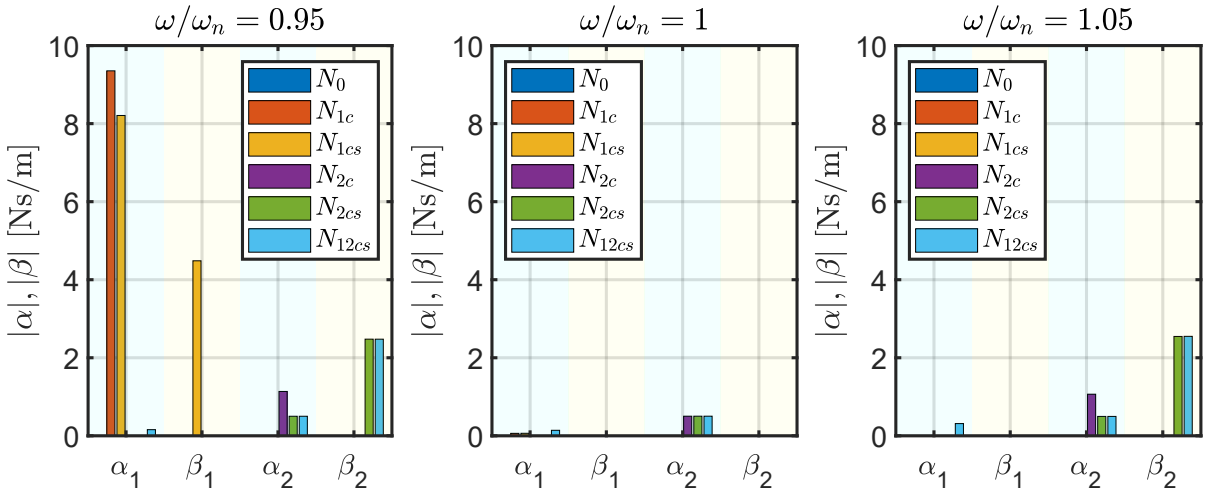

Figure 9: Optimized control parameters.

on the system. Figure 10 shows the peak absolute velocity ($\hat{z}$) and peak absolute PTO force ($\hat{F}$), for each control law. Promptly evident is the velocity magnification of first-order strategies at $\omega < \omega_n$, mainly achieved by driven power provided by the PTO; in fact, the large PTO force coefficients, shown in Fig. 9, combined with such large velocities, produce the large forces shown in Fig. 10. In other words, first-order control strategies aim at feeding a large quantity of energy into the system in order to increase the velocity, as also shown in the time traces in Fig. 5. Conversely, the forces imposed by second-order control laws are significantly lower than first-order, although higher than N_0; the obtained optimal velocity profile of N_{2cs} closely follows the trend of the excitation force magnitude, proportional to ω^2. The velocity trend of N_{2c}, being 'incomplete' of the sine term, follows the optimal profile imperfectly.

An ultimate, likely the most important, metric that guides the design of an energy harvester is the cost. A reasonably good proxy for the cost of the transducer is the maximum force it is able to exert. If so, according to Fig. 10, first-order control laws would be the most demanding. However, a major cost driver often is the ability of the PTO mechanism to feed power directly into the system, required to enable optimal active control. Semi-active control strategies, although potentially suboptimal, are likely to be less expensive. Therefore, it is crucial to quantify the marginal gain in power extraction of optimal active control with respect to suboptimal semi-active control, in order to evaluate if the increase in cost is justifiable. Therefore, a constrained optimization is performed, requiring the instantaneous power to be always positive (passivity constraint), obtaining the optimal mean semi-active power ($\overline{P}^{sa}$). Figure 11 shows $\overline{P}^{sa}$ in absolute value in the top-left graph, and compares it to the best mean active power for each control strategy ($\overline{P}^{a}$) in the bottom-left graph, to the best overall $\overline{P}^{sa}$ ($\overline{P}^{sa}_{opt}$) in the top-right graph, and to the best overall $\overline{P}^{a}$ ($\overline{P}^{a}_{opt}$) in the bottom-right graph.

Overall, differences between semi-active control strategies are reduced, all following the bell-shape of the LTI system. First-order control is not able to bring any improvement from the N_0 even at $\omega < \omega_n$, confirming the full reliance on drive power. On the other hand, with the passivity constraint, N_0 power output is between 70% and 91% of the best semi-active control, while the comparison with the best active control abruptly drops down to 7%.

Second-order control laws, differently from first order, are shown able to achieve performance

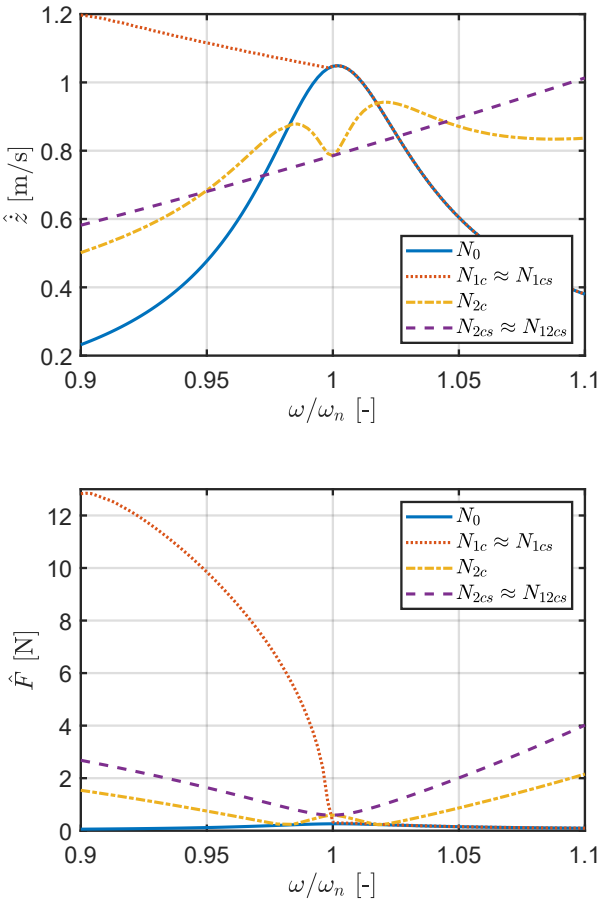

Figure 10: Peak absolute velocity ($\hat{z}$) and peak absolute PTO force ($\hat{F}$).

improvement also with the passivity constraint. It is worthwhile to notice that semi-active N_{2c} performs exactly as well as active N_{2c} within the frequency range between 97% and 103% of ω_n. However, in such a range, the power output is down to 80% the best semi-active power obtained with N_{2cs}, while interestingly improve up to 100% further away from resonance. Similarly, it is also interesting to remark that the sine term is the one affecting the most the active power flow, since the performance degradation of semi-active N_{2cs} with respect to its active version is greater than the one experienced by N_{2c}.

Nevertheless, from all plots in Fig. 11, it is clear that N_{2cs} outperforms all other strategies even when the passivity constraint is included. On the other hand, the performance of semi-active optimal control is significantly lower than the active control, with a 60% drop already at a frequency 5% away from ω_n.

6. Conclusions

This paper tackles the problem of performance enhancement of a vibration energy harvesting via time variations of the power take-off (PTO) damping coefficient: the PTO force, proportional to the velocity by means of the damping coefficient, is used to both extract energy and modify

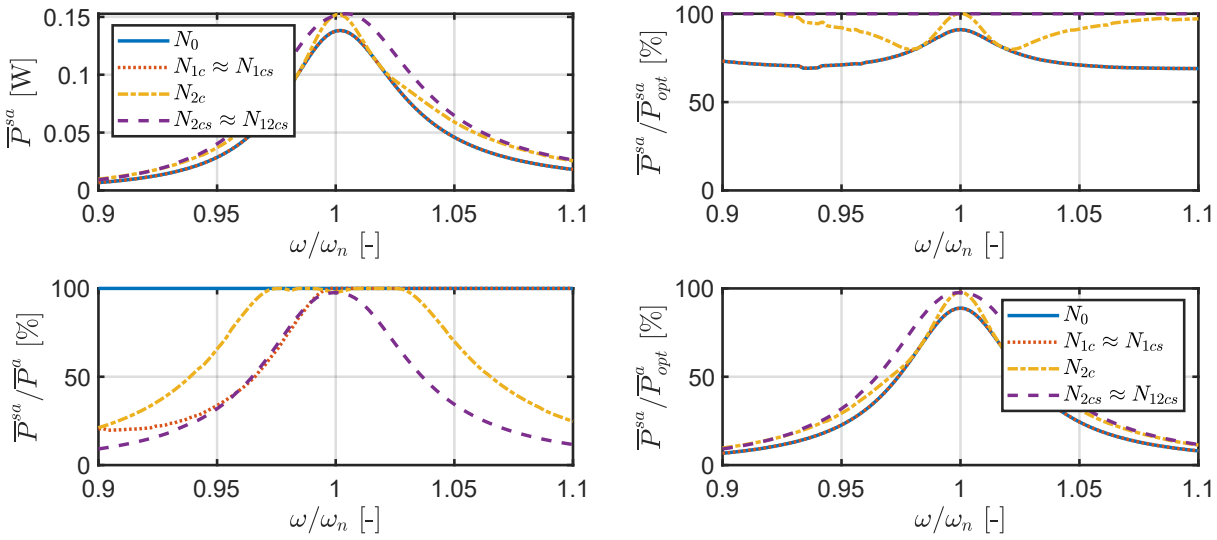

Figure 11: Mean semi-active power ($\overline{P}^{sa}$) in the top-left graph, compared to the best mean active power for each control strategy ($\overline{P}^{a}$) in the bottom-left graph, to the best overall $\overline{P}^{sa}$ ($\overline{P}^{sa}_{opt}$) in the top-right graph, and to the best overall $\overline{P}^{a}$ ($\overline{P}^{a}_{opt}$) in the bottom-right graph.

the system dynamics. The analysis, optimization and simulation of linear time variant systems, generally challenging, is efficiently performed in this paper via a rigorous mathematical framework based on pseudospectral decomposition. Such a general mathematical framework, applicable to other classes of LTV systems, also with different or no parametrization of the control force, is first used to set assumptions and conditions for the existence of solutions to the so-called steady-state optimal control problem, including an algebraic computation of the steady-state response associated with the energy harvester. With such a simulation tool, an extensive analysis of harmonic parametrization of the PTO coefficient is performed, founding that the best solution, in terms of power extraction, is obtained with a PTO coefficient varying at twice the excitation frequency, including both orthogonal harmonic basis (*i.e.* both sine and cosine, N_{2cs}), while lower and higher harmonics are deemed redundant. Admitting bidirectional power flow at the PTO, N_{2cs} extremely enlarges the bandwidth, while keeping both velocity and PTO control force relatively low, similar in magnitude to the uncontrolled case, hence without posing unacceptable additional stress on the system that would hinder a smooth implementation. Furthermore, if a monodirectional PTO system has to be used, due to specific design or cost constraints, the semi-active N_{2cs} still outperforms other control laws considered, bringing a significant bandwidth magnification. However, the power extraction of the semi-active approach is greatly lower than the active approach, so additional costs for bidirectional transducers should be carefully taken into account in light of the marginal gain in productivity.

Appendix A. Proof of proposition 1

Let $\tilde{A} : \mathbb{R}^+ \to \mathbb{R}^{2\times 2}$ be defined such that

$$\tilde{A}(t) = \begin{bmatrix} 0 & 1 \\ -c_d/m & -(c_d + b^0_{\mathrm{PTO}} + b_{\mathrm{PTO}}(t))/m \end{bmatrix}. \tag{A.1}$$

The input-to-state equation in (10) can be conveniently written in terms of (A.1) as

$$\dot{\varphi} = \tilde{A}(t)\varphi + Bf_e, \tag{A.2}$$

where, given the T_0-periodicity of b_{PTO}, it is straightforward to note that the matrix $\tilde{A}(t)$ is such that $\tilde{A}(t) = \tilde{A}(t - T_0)$, *i.e.* is periodic with the same period as the exciting force f_e (input to the system). In other words, system (A.2) is a *periodic* LTV system, where the period of the time-varying matrices involved exactly coincides with that of the input. Then, the proof of the claim directly follows from Floquet's stability theory for periodic systems (see, for instance, [41, Theorem 3.4]): If Assumption 1 holds, the steady-state response of system (A.2) driven by the input f_e is always well-defined and T_0-periodic, *i.e.* $\varphi^{ss}(t) = \varphi^{ss}(t - T_0)$.

Appendix B. Proof of proposition 2

Note that, since the set $\{t_j\} \subset \Xi_0$, and that each entry of the residual mapping is continuous on Ξ_0, then $\langle \mathcal{R}, \delta_{t_j} \rangle = \mathcal{R}(t_j)$, for all $j \in \mathbb{N}_{2M}$. Finally, the result follows as a consequence of the fact that the entries of $\xi_M(t)$ constitute a set of persistently exciting signals, which directly implies that the matrix Ω is always full rank [42], *i.e.* Ω^{-1} is well-defined.

Appendix C. Proof of proposition 3

We first introduce an important definition, required to provide a proof of Proposition 3.

Definition 3 (Kronecker sum)**.** [32] The *Kronecker sum* of two matrices P_1 and P_2, with $P_1 \in \mathbb{R}^{n\times n}$ and $P_2 \in \mathbb{R}^{k\times k}$, is defined (and denoted) as

$$P_1 \hat{\oplus} P_2 \triangleq P_1 \otimes \mathbb{I}_k + \mathbb{I}_n \otimes P_2. \tag{C.1}$$

A direct application of the vec operator (as in Definition 1) to equation (20), together with Property 2, yields:

$$\mathcal{W}(\bar{B}_{\mathrm{PTO}})\,\mathrm{vec}\{\bar{\Phi}\} = (\mathbb{I}_{2M} \otimes (-B))\mathrm{vec}\{\bar{F}_e\}, \tag{C.2}$$

where the matrix $\mathcal{W}(\bar{B}_{\mathrm{PTO}}) \in \mathbb{R}^{4M\times 4M}$ is defined as

$$\mathcal{W}(\bar{B}_{\mathrm{PTO}}) = (A \otimes \mathbb{I}_{2M}) - (S^{\intercal} \otimes \mathbb{I}_2) - ((\mathcal{M}(\bar{B}_{\mathrm{PTO}})\Omega^{-1})^{\intercal} \otimes BC). \tag{C.3}$$

It is then clear that existence and uniqueness of the solution of (20) can be guaranteed as long as $0 \notin \lambda(\mathcal{W}(\bar{B}_{\mathrm{PTO}}))$. Following Definition 3, it is straightforward to note that $\mathcal{W}(\bar{B}_{\mathrm{PTO}})$ can be written in terms of an appropriate *Kronecker sum* (see Definition 3), *i.e.*

$$\mathcal{W}(\bar{B}_{\mathrm{PTO}}) = (A + BC)\,\hat{\oplus}\,(-S^{\intercal} - (\mathcal{M}(\bar{B}_{\mathrm{PTO}})\Omega^{-1})^{\intercal}), \tag{C.4}$$

whose eigenvalues can be computed (by means of Property 1) as $\lambda(A+BC)-\lambda(S^{\intercal}+(\mathcal{M}(\bar{B}_{\mathrm{PTO}})\Omega^{-1})^{\intercal})$, where the operator "$-$" in this context denotes the Minkowski difference of two sets. In other words, the inverse of $\mathcal{W}(\bar{B}_{\mathrm{PTO}})$ is well-defined as long as the spectra of $A + BC$ and[4] $S + \mathcal{M}(\bar{B}_{\mathrm{PTO}})$ are disjoint, which, since this is the case by Assumption 2, the claim follows.

[4]Note that the spectra of a matrix coincides with that of its transpose.

Appendix D. Proof of proposition 4

Note that the integral term in (22) can be conveniently written[5] as

$$\bar{J} = \frac{1}{T_0} C\bar{\Phi} \left[\int_{\Xi_0} \xi_M(\tau) \left(b^0_{\mathrm{PTO}} + \bar{B}_{\mathrm{PTO}} \xi_M \right) \xi_M^\intercal d\tau \right] \left(C\bar{\Phi} \right)^\intercal \tag{D.1}$$

Since $\bar{J} \in \mathbb{R}$, a direct application of the vec operator (as in Definition 1), together with Property 2, yields

$$\bar{J} = \bar{J}^\intercal = \mathrm{vec}\{\bar{J}\} = \frac{1}{T_0} \left(C\bar{\Phi} \otimes C\bar{\Phi} \right) \mathrm{vec} \left\{ \int_{\Xi_0} \xi_M \left(b^0_{\mathrm{PTO}} + \bar{B}_{\mathrm{PTO}} \xi_M \right) \xi_M^\intercal d\tau \right\}. \tag{D.2}$$

Since the vec operator is a linear map by definition, it is straightforward to check that (D.2) can be further simplified as

$$\begin{aligned} \bar{J} &= \frac{1}{T_0} \left(C\bar{\Phi} \otimes C\bar{\Phi} \right) \left[\int_{\Xi_0} b^0_{\mathrm{PTO}} \left(\xi_M \otimes \xi_M \right) + \left(\xi_M \xi_M^\intercal \otimes \xi_M^\intercal \right) \mathrm{vec}\{\bar{B}_{\mathrm{PTO}}\} d\tau \right] = \\ &= \frac{1}{T_0} \left(C\bar{\Phi} \otimes C\bar{\Phi} \right) \left[b^0_{\mathrm{PTO}} \mathcal{X}_1 + \mathcal{X}_2 \bar{B}^\intercal_{\mathrm{PTO}} \right], \end{aligned} \tag{D.3}$$

where the last equality follows by noting that $\mathrm{vec}\{\bar{B}_{\mathrm{PTO}}\} = \bar{B}^\intercal_{\mathrm{PTO}}$. Finally, from equation (C.2), the following relation

$$\mathrm{vec}\{C\bar{\Phi}\} = (\mathbb{I}_{2M} \otimes C)\mathrm{vec}\{\bar{\Phi}\} = (\mathbb{I}_{2M} \otimes C)\mathcal{W}(\bar{B}_{\mathrm{PTO}})^{-1}(\mathbb{I}_{2M} \otimes (-B))\mathrm{vec}\{\bar{F}_e\}, \tag{D.4}$$

holds, since the inverse of $\mathcal{W}(\bar{B}_{\mathrm{PTO}})$ is always well-defined by virtue of Assumption 2. Note now that $\mathrm{vec}\{C\bar{\Phi}\} = (C\bar{\Phi})^\intercal$ and $\mathrm{vec}\{\bar{F}_e\} = \bar{F}_e^\intercal$, and hence the equality $C\bar{\Phi} = \bar{F}_e \bar{\mathcal{W}}(\bar{B}_{\mathrm{PTO}})$, with $\bar{\mathcal{W}}(\bar{B}_{\mathrm{PTO}})$ as in equation (24), stems directly from (D.4), which proves the claim.

References

[1] Zheng, Q., Shi, B., Li, Z., Wang, Z.L.. Recent Progress on Piezoelectric and Triboelectric Energy Harvesters in Biomedical Systems. Advanced Science 2017;4(7):1700029. doi:10.1002/advs.201700029.

[2] Benchemoul, M., Ferin, G., Rosinski, B., Bantignies, C., Hoang, T., Vince, P., et al. Wireless Inertial Sensing Platform Self-Powered by Piezoelectric Energy Harvester for Industrial Predictive Maintenance. In: IEEE International Ultrasonics Symposium, IUS; vol. 2018-Octob. IEEE Computer Society. ISBN 9781538634257; 2018,doi:10.1109/ULTSYM.2018.8580029.

[3] Guo, F., Hayat, H., Wang, J.. Energy harvesting devices for high voltage transmission line monitoring. In: IEEE Power and Energy Society General Meeting. ISBN 9781457710018; 2011,doi:10.1109/PES.2011.6039037.

[4] Shaikh, F.K., Zeadally, S.. Energy harvesting in wireless sensor networks: A comprehensive review. 2016. doi:10.1016/j.rser.2015.11.010.

[5] Jeong, B., Kim, M.O., Lee, J.I., Eun, Y., Choi, J., Kim, J.. Development of MEMS Multi-Mode Electrostatic Energy Harvester Based on the SOI Process. Micromachines 2017;8(2):51. doi:10.3390/mi8020051.

[6] Ji, B., Chen, Z., Chen, S., Zhou, B., Li, C., Wen, H.. Joint optimization for ambient backscatter communication system with energy harvesting for IoT. Mechanical Systems and Signal Processing 2020;135:106412. doi:10.1016/j.ymssp.2019.106412.

[7] Siddique, A.R.M., Mahmud, S., Heyst, B.V.. A comprehensive review on vibration based micro power generators using electromagnetic and piezoelectric transducer mechanisms. 2015. doi:10.1016/j.enconman.2015.09.071.

[5] Note that we omit the dependence on t in the integral operations throughout this proof, to simplify the notation.

[8] Ali, S.F., Friswell, M.I., Adhikari, S.. Analysis of energy harvesters for highway bridges. Journal of Intelligent Material Systems and Structures 2011;22(16):1929–1938. doi:10.1177/1045389X11417650.
[9] Rojas, R.A., Carcaterra, A.. An approach to optimal semi-active control of vibration energy harvesting based on MEMS. Mechanical Systems and Signal Processing 2018;107:291–316. doi:10.1016/j.ymssp.2017.11.005.
[10] Zou, D., Liu, G., Rao, Z., Tan, T., Zhang, W., Liao, W.H.. A device capable of customizing nonlinear forces for vibration energy harvesting, vibration isolation, and nonlinear energy sink. Mechanical Systems and Signal Processing 2021;147:107101. doi:10.1016/j.ymssp.2020.107101.
[11] Siang, J., Lim, M.H., Salman Leong, M.. Review of vibration-based energy harvesting technology: Mechanism and architectural approach. International Journal of Energy Research 2018;42(5):1866–1893. doi:10.1002/er.3986.
[12] Jia, Y.. Review of nonlinear vibration energy harvesting: Duffing, bistability, parametric, stochastic and others. Journal of Intelligent Material Systems and Structures 2020;31(7):921–944. doi:10.1177/1045389X20905989.
[13] Bahrami, A., Tayarani, M.. Chaotic Behavior of Duffing Energy Harvester. Energy Harvesting and Systems 2018;5(3-4):67–71. doi:10.1515/ehs-2018-0011.
[14] Liu, D., Wu, Y., Xu, Y., Li, J.. Stochastic response of bistable vibration energy harvesting system subject to filtered Gaussian white noise. Mechanical Systems and Signal Processing 2019;130:201–212. doi:10.1016/j.ymssp.2019.05.004.
[15] Giorgi, G., Gomes, R.P.F., Bracco, G., Mattiazzo, G.. Numerical investigation of parametric resonance due to hydrodynamic coupling in a realistic wave energy converter. Nonlinear Dynamics 2020;doi:10.1007/s11071-020-05739-8.
[16] McInnes, C.R., Gorman, D.G., Cartmell, M.P.. Enhanced vibrational energy harvesting using nonlinear stochastic resonance. Journal of Sound and Vibration 2008;318(4-5):655–662. doi:10.1016/j.jsv.2008.07.017.
[17] Scruggs, J.T.. An optimal stochastic control theory for distributed energy harvesting networks. Journal of Sound and Vibration 2009;320(4-5):707–725. doi:10.1016/j.jsv.2008.09.001.
[18] Cassidy, I.L., Scruggs, J.T.. Nonlinear stochastic controllers for power-flow-constrained vibratory energy harvesters. Journal of Sound and Vibration 2013;332(13):3134–3147. doi:10.1016/j.jsv.2013.01.023.
[19] Wickenheiser, A.M., Garcia, E.. Power Optimization of Vibration Energy Harvesters Utilizing Passive and Active Circuits. Journal of Intelligent Material Systems and Structures 2010;21(13):1343–1361. doi:10.1177/1045389X10376678.
[20] Qiu, J.H., Ji, H.L., Shen, H.. Energy harvesting and vibration control using piezoelectric elements and a nonlinear approach. IEEE International Symposium on Applications of Ferroelectrics 2009;doi:10.1109/ISAF.2009.5307559.
[21] Scapolan, M., Tehrani, M.G., Bonisoli, E.. Energy harvesting using parametric resonant system due to time-varying damping. Mechanical Systems and Signal Processing 2016;79:149–165. doi:10.1016/j.ymssp.2016.02.037.
[22] Cassidy, I.L., Scruggs, J.T.. Statistically linearized optimal control of an electromagnetic vibratory energy harvester. Smart Materials and Structures 2012;21(8). doi:10.1088/0964-1726/21/8/085003.
[23] Rojas, R.A., Carcaterra, A.. An approach to optimal semi-active control of vibration energy harvesting based on MEMS. Mechanical Systems and Signal Processing 2018;107:291–316. doi:10.1016/j.ymssp.2017.11.005.
[24] Liu, Y., Matsuhisa, H., Utsuno, H.. Semi-active vibration isolation system with variable stiffness and damping control. Journal of Sound and Vibration 2008;313(1-2):16–28. doi:10.1016/j.jsv.2007.11.045.
[25] Di Monaco, F., Ghandchi Tehrani, M., Elliott, S.J., Bonisoli, E., Tornincasa, S.. Energy harvesting using semi-active control. Journal of Sound and Vibration 2013;332(23):6033–6043. doi:10.1016/j.jsv.2013.06.005.
[26] Hurlebaus, S., Gaul, L.. Smart structure dynamics. Mechanical Systems and Signal Processing 2006;20(2):255–281. doi:10.1016/j.ymssp.2005.08.025.
[27] Giorgi, G.. PARAMETRIC RESONANCE EXPLOITATION DUE TO PERIODIC DAMPING IN AN ELECTROMECHANICAL ENERGY HARVESTER. International Journal of Mechanics and Control 2021;22(01):77–85.
[28] Faedo, N., Scarciotti, G., Astolfi, A., Ringwood, J.V.. On the Approximation of Moments for Nonlinear Systems. IEEE Transactions on Automatic Control 2021;doi:10.1109/tac.2021.3054325.
[29] Faedo, N., Scarciotti, G., Astolfi, A., Ringwood, J.V.. Nonlinear Energy-Maximizing Optimal Control of Wave Energy Systems: A Moment-Based Approach. IEEE Transactions on Control Systems Technology 2021;doi:10.1109/TCST.2020.3047229.
[30] Ross, I.M., Karpenko, M.. A review of pseudospectral optimal control: From theory to flight. Annual Reviews in Control 2012;36(2):182–197.
[31] Genest, R., Ringwood, J.V.. Receding horizon pseudospectral control for energy maximization with application to wave energy devices. IEEE Transactions on Control Systems Technology 2016;25(1):29–38.

[32] Brewer, J.W.. Kronecker Products and Matrix Calculus in System Theory. IEEE Transactions on Circuits and Systems 1978;25(9):772–781. doi:10.1109/TCS.1978.1084534.
[33] Khalil, H.K.. Nonlinear Systems. Third ed.; Upper Saddle River, NJ: Prentice Hall; 2002. ISBN 0130673897, 9780130673893. doi:10.1016/j.physa.2006.08.011.
[34] Finlayson, B., Scriven, L.. The method of weighted residuals—a review. Applied Mechanics Review 1966;19(9):735–748.
[35] Boyd, J.P.. Chebyshev and Fourier Spectral Methods Second Edition. Tech. Rep.; 2001.
[36] Waltz, R.A., Morales, J.L., Nocedal, J., Orban, D.. An interior algorithm for nonlinear optimization that combines line search and trust region steps. Mathematical Programming 2006;107(3):391–408. doi:10.1007/s10107-004-0560-5.
[37] Forsgren, A., Gill, P.E., Wright, M.H.. Interior methods for nonlinear optimization. SIAM review 2002;44(4):525–597.
[38] Byrd, R.H., Hribar, M.E., Nocedal, J.. An interior point algorithm for large-scale nonlinear programming. SIAM Journal on Optimization 1999;9(4):877–900.
[39] García-Violini, D., Faedo, N., Jaramillo-Lopez, F., Ringwood, J.V.. Simple controllers for wave energy devices compared. Journal of Marine Science and Engineering 2020;8(10):1–30. doi:10.3390/jmse8100793.
[40] Yurchenko, D., Alevras, P., Zhou, S., Wang, J., Litak, G., Gaidai, O., et al. Nonlinear vibration mitigation of a crane's payload using pendulum absorber. Mechanical Systems and Signal Processing 2021;156:107558. doi:10.1016/j.ymssp.2020.107558.
[41] Wereley, N.M.. Analysis and control of linear periodically time varying systems. Ph.D. thesis; Massachusetts Institute of Technology; 1990.
[42] Padoan, A., Scarciotti, G., Astolfi, A.. A Geometric Characterization of the Persistence of Excitation Condition for the Solutions of Autonomous Systems. IEEE Transactions on Automatic Control 2017;62(11):5666–5677. doi:10.1109/TAC.2017.2687760.